


# Improvement the mode I interlaminar fracture toughness of glass fiber reinforced phenolic resin by using epoxidized soybean oil

Cuong Manh Vu<sup>1,2</sup>  · Dinh Duc Nguyen<sup>3,4</sup> · Le Hoang Sinh<sup>3</sup> · Hyoung Jin Choi<sup>5</sup> · Tien Duc Pham<sup>6</sup>

Received: 8 September 2017 / Revised: 12 December 2017 / Accepted: 19 February 2018 /  
Published online: 23 February 2018  
© Springer-Verlag GmbH Germany, part of Springer Nature 2018

**Abstract** In this study, the epoxidized soybean oil (ESO) was successfully synthesized from soybean oil based on its double bond, and used to synthesize the ESO-modified phenolic resin via reaction between ESO, phenol and formaldehyde. The ESO contents used in this study vary in range from 0 to 40 wt%. Then, the obtained ESO modified phenolic resin (ESO-PR) was used as resin matrices to fabricate glass-fiber-based composites by using prepreg technique. The chemical structures of both epoxidized soybean oil and phenolic resin modified with epoxidized soybean oil were confirmed with the help of Fourier transform infrared spectrometry (FTIR). The mechanical characteristics of fabricated composite materials examined include the tensile property, flexural property, impact property as well as the mode I interlaminar fracture toughness, while the morphology composite materials were also confirmed by scanning electron microscopy. The test results showed that at 20 wt% of ESO-PR, the mode I interlaminar fracture toughness for both propagation and initiation, the tensile strength, flexural strength and impact strength were

---

✉ Cuong Manh Vu  
vumanhcuong1@tdt.edu.vn

✉ Dinh Duc Nguyen  
nguyensyduc@gmail.com

<sup>1</sup> Department for Management of Science and Technology Development, Ton Duc Thang University, Ho Chi Minh City, Vietnam

<sup>2</sup> Faculty of Applied Sciences, Ton Duc Thang University, Ho Chi Minh City, Vietnam

<sup>3</sup> Institute of Research and Development, Duy Tan University, Da Nang, Vietnam

<sup>4</sup> Department of Environmental Energy and Engineering, Kyonggi University, Suwon 442-760, Korea

<sup>5</sup> Department of Polymer Science and Engineering, Inha University, Incheon 22212, Korea

<sup>6</sup> Faculty of Chemistry, Hanoi University of Science, Vietnam National University, Hanoi, 19 Le Thanh Tong, Hoan Kiem, Hanoi 10000, Vietnam

increased by 78.3 and 84.5%, 7.0%; 20.5 and 39.7%, respectively. The scanning electron microscopy (SEM) observation indicated that the fracture surface of the modified composite was rougher when compared to the fracture surface of the pristine composite, and hence more energy was needed for the crack to propagate.

**Keywords** Epoxidized soybean oil · Resole-type phenolic resin · Mode I interlaminar fracture toughness · Mechanical properties

## Introduction

Phenolic resin (PR), a traditional resin, is the condensed product of phenol and formaldehyde and has been widely used in different industries such as, adhesives, coatings, wood binders, and laminates for a long time due to its excellent features such as, thermal resistance, dimensional stability, and flame retardation [1]. However, the pristine phenolic resin have showed many disadvantages such as brittleness, high curing temperature, and too high/low viscosity that they can hardly being applied in some high technology areas such as carbon based composites, high strength electronic devices, etc [2]. Many methods have been applied to improve the toughness of pristine PR either by using porous particles [3], functionalized silica sols [4], diacids [5], boron [6], rubber [7, 8] or silicone [9–11] or change the curing mechanism from condensation polymerization to additional polymerization [12]. Hengyi Ma et al. [13] used organic elastomeric nanoparticles including nitrile butadiene and carboxylic nitrile butadiene rubbers to modify PR. The fabricated phenolic resin nanocomposite exhibited excellent impact strength, flexural strength and heat resistance. Cevdet Kaynak et al. [7] used nitrile rubber and amino silane to toughen phenolic resin. The results showed that the modification by using nitrile rubber and amino silane together was much more effective than by using only nitrile rubber. Megiatto Jr. et al. [14] investigated the toughening of phenolic thermoset and its composites reinforced with sisal fibers, using hydroxyl-terminated polybutadiene rubber (HTPB) as both impact modifier and coupling agent. The use of nanofillers can be considered as the best way to enhance the fracture toughness and mechanical properties of phenolic resin based on the last obtained results from thermoset resin [15–17].

Because of many environmental benefits, the renewable and sustainable tougheners have been attracting many researchers from around the world and increasing to use for enhancement the properties of thermoset resins [18–21]. The toughener based on plant oils has emerged as an effective modifier for either phenol resin or other thermoset resin [22–26]. The novelty of this study is focusing on both synthesis of epoxidized soybean oil and using as toughner for phenolic resin, phenolic resin based glass fiber composite.

In this study, we examine whether epoxidized soybean oil (ESO) is applicable to PR for modifying the matrix of glass fiber/PR composites. It is also one of the objectives to quantitatively determine as to what extent the mechanical properties are improved in tensile strength, impact strength and mode I interlaminar fracture

toughness. ESO was synthesized from soybean oil based on double bond via epoxidation reaction.

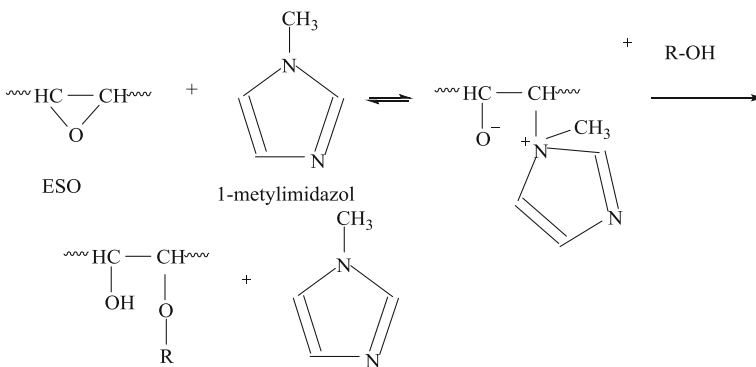
## Experimental section

### Materials

Phenol (99%), formalin (37%), ammonia (25%) were obtained from Sigma-Aldrich (USA). 1-Methylimidazole (NMI) was purchased from BASF (Singapore) to play a catalyst role for reaction between hydroxyl group and epoxy group (Scheme 1). Soybean oil (SO) was supplied by Cai Lan Oil and Fats Industries Co. Ltd (Vietnam). Ethanol (99%), formic acid (98%), hydrogen peroxide (30%) and cloth glass fiber were procured from Tianjin Chemicals (China).

### Epoxidation process

Soybean oil and formic acid were added to a three-necked reaction flask fitted with a mechanical stirrer and a thermometer along with a reflux condenser. The reaction mixture was stirred at 1000 rpm at 50 °C for 20 min. Further, for the initiation of the epoxidation, calculated amount of 30% aqueous hydrogen peroxide was added drop-wise to the above reaction mixture for 1 h. In this reaction, formic acid acts as an active oxygen carrier and hydrogen peroxide as an oxygen donor to form in situ peroxyformic acid, which gave the product ESO (Fig. 1). The addition of hydrogen peroxide should be slow, to avoid the possibility of explosion. After complete addition of hydrogen peroxide, stirring was continued for 5 h at 50 °C to complete the reaction. Afterwards, the reaction mixture was cooled to room temperature and washed with water to remove excess acid. ESO was further dried with anhydrous sodium sulphate and kept in oven at 65 °C for 12 h. The oxirane content (6.1%) was



**Scheme 1** Proposed reaction mechanism between ESO and PR

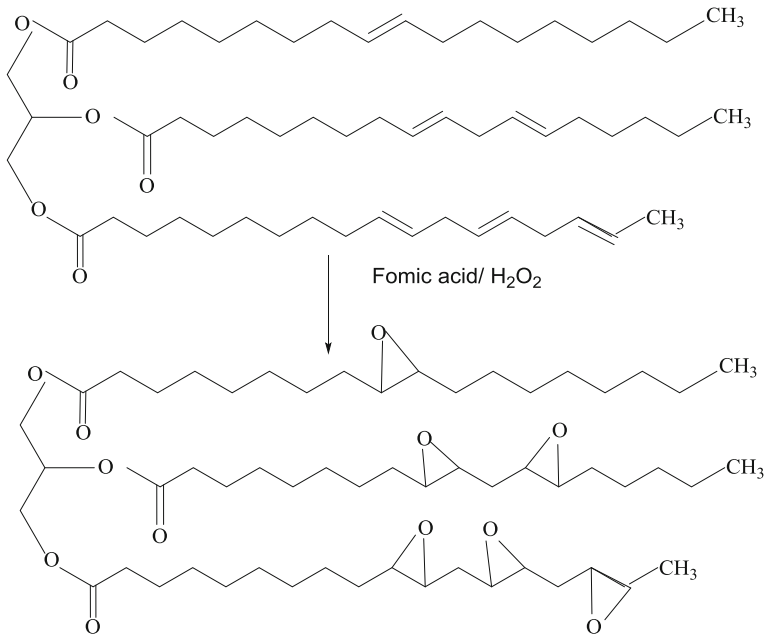


**Fig. 1** Epoxidation reaction of soybean oil

determined by titration method with direct 0.1 N hydrobromic acid solutions in glacial acetic acid.

### Synthesis of the epoxidized soybean oil-modified phenolic resins (ESO-PR)

The epoxidized soybean oil-modified phenolic resins (ESO-PR) prepared with contents of epoxidized linseed oil varied from 0 to 40% by weight in comparison with the sum of phenol and formaldehyde. The reactions were carried out in a glass flask equipped with a magnetic stirrer, a condenser and heating equipment. Briefly, 70.0 g phenol (98%), 72.4 g formalin (37%) and 3.5 g NH<sub>3</sub> (25%) were charged to a 250 ml capacity of three-necked flask. The temperature was increased from room temperature to around 60 °C while stirring and was kept for about 30 min. After that, ESO in a specific content, and NMI 0.15% in comparison with the sum of phenol and formaldehyde were also added to reactor. The temperature was maintained at 60 °C for 30 min. In the next step, the temperature of the reaction was increased to 90–95 °C and kept for about 90 min. Finally, the products were poured into a ceramic bowl, washed several times with water and dried at 70 °C under vacuum. The finished products obtained with liquid state had light yellow color.

In order to synthesis phenolic resin the analog procedure was applied with absence of both ESO and NMI.

## Composite preparation

Composite materials based on PR and PR-ESO reinforced with glass fiber were prepared by prepreg method with the resin/fiber weight ratio was 60/40. Resin was dissolved in acetone to get the certain concentrations then was impregnated into the glass fiber. The prepreg sheets were placed in air at room temperature for about 10–15 h to remove all the solvent.

The prepreg sheets then were stacked in a steel mold and pressed at 150 °C for 30 min prior to receive the final composite materials.

## Characterization techniques

The morphology of the composite materials was examined with a JEOL JSM-6360 (Japan) scanning electron microscope (SEM). Prior to the SEM observations, all the samples were coated with a thin layer of platinum to avoid the build-up of an electrical charge.

The attenuated total reflectance of FTIR spectra were acquired at 25 °C on a PerkinElmer Spectrum One spectrometer equipped with a Universal ATR sampling accessory (diamond crystal) and a red laser excitation source (632.8 nm). Spectra were recorded in the range between 4000 and 400  $\text{cm}^{-1}$ .

The thermal stability of the composites was analyzed by TGA using a Setaram TG (France) at a heating rate of 10 °C/min. The temperature was scanned from room temperature to 550 °C under a nitrogen atmosphere, with a purge gas flow rate of 60 mL/min.

Tensile properties were measured with an Instron 5582-100 kN (USA) mechanical tester at  $23 \pm 2$  °C and  $50 \pm 5\%$  RH, using a crosshead speed of 2 mm/min, according to the ISO 527-1 standard. Five specimens for each type of composite were measured.

Flexural properties were measured with an Instron 5582-100 kN (USA) mechanical tester at  $23 \pm 2$  °C and  $50 \pm 5\%$  RH, using a crosshead speed of 2 mm/min, according to the ISO 178 standard. Five specimens for each type of composite were measured.

Izod impact strength tests were carried out on a Tinius Olsen Model 92T (USA) impact tester, according to the ISO 180 standard. Measurements were performed at  $23 \pm 2$  °C and  $50 \pm 5\%$  RH. The data correspond to the average value of seven specimens.

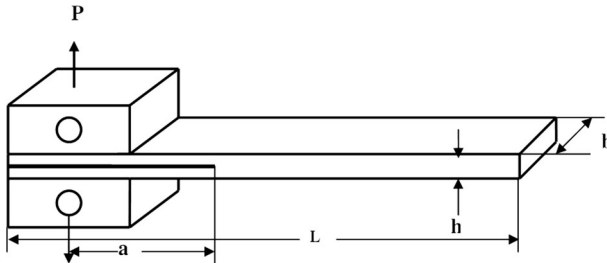
To measure the mode-I interlaminar fracture toughness, a mode I double-cantilever beam test was carried out as described in ASTM: D5528-01. This standard recommends a specimen size of at least 150 mm (L) by 20 mm (W) with an initial crack length (i.e. the length of the insert from the line) of 50 mm. Hinges of the same width as the specimen were attached to allow the application of the load. The load and displacement were then related to the delamination length as measured with a ruler at the specimen edge. The mode-I interlaminar fracture toughness  $G_{IC}$  and  $G_{IP}$  for each ESO content were calculated using the modified compliance calibration method and Eqs. (1) and (2):

$$G_{IC} = \frac{3m}{2(2h)} \cdot \left(\frac{P_c}{B}\right)^2 \cdot \left(\frac{BC}{N}\right)^{\frac{2}{3}} F \quad (1)$$

$$G_{IP} = \frac{3m}{2(2h)} \cdot \left(\frac{P_p}{B}\right)^2 \cdot \left(\frac{BC}{N}\right)^{\frac{2}{3}} F \quad (2)$$

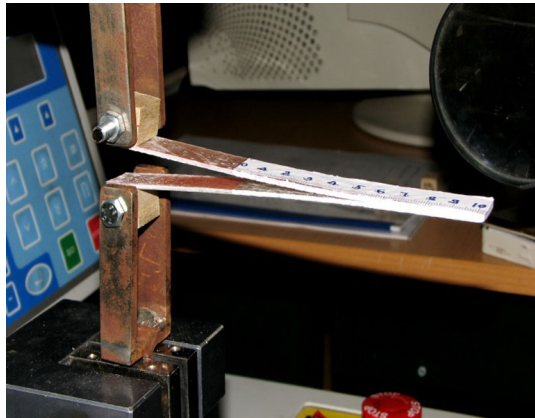
where  $G_{IC}$  is the fracture toughness at the initial crack stage,  $G_{IP}$  is the fracture toughness at the propagation stage,  $P_p$  is the applied load,  $C$  is the compliance corresponding to each crack length,  $a$  is the crack length,  $P_c$  is the initial maximum load,  $B$  is the specimen width,  $2h$  is the thickness in equation,  $N$  is the end-block correction factor,  $F$  is the large-displacement correction factor, and  $m$  is the slope of a plot of  $(BC/N)^{1/3}$  versus  $(a/2h)$ .

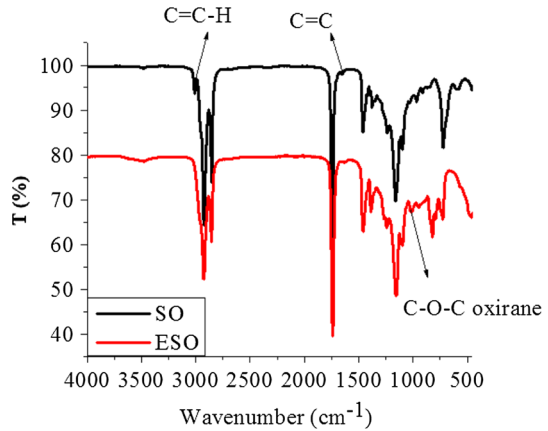
The sample dimensions and testing processing can be seen in Figs. 2 and 3.



**Fig. 2** Geometry of DCB specimen (all dimensions in mm:  $L = 150$ ;  $h = 4$ ;  $b = 20$ ;  $a = 50$ )

**Fig. 3** Picture of interlaminar fracture toughness testing



**Fig. 4** FTIR spectra of SO and ESO

## Results and discussion

### FTIR studies

The FTIR spectra of SO and uncured ESO were compared in Fig. 4 to confirm the success of epoxidation reaction. SO presents intense signals at 1744 and 1160  $\text{cm}^{-1}$  related to the C=O and C–O stretching, respectively, in triglyceride molecules [27]. The peaks at 2925 and 2860  $\text{cm}^{-1}$  arise from the asymmetric and symmetric C–H stretching in methylene groups, while their asymmetric and symmetric bending appears at 1460 and 1380  $\text{cm}^{-1}$ , respectively, and the bands at 3020, 1650, and 720  $\text{cm}^{-1}$  respectively correspond to stretching vibrations of double bonds: =C–H, C=C, and cis CH=CH. New signals can be observed in the spectrum of uncured ESO at 1240, 828, and 780  $\text{cm}^{-1}$  referred to different C–O–C stretching modes of the oxirane ring [28], together with the disappearance of the bands at 3020 and 1650  $\text{cm}^{-1}$ , thus corroborating the success of the epoxidation reaction. The bands related to the epoxy group are hardly visible in the spectrum of the cured ESO, simultaneous with the increase of the intensity of a band at  $\sim 1100 \text{ cm}^{-1}$  related to the C–O stretching of the ether group that overlaps with the C–O vibration of the triglycerides.

Figure 5 shows the FTIR spectra of the samples: unmodified PR (1) and cPR-ESO (2). The bands at 3414  $\text{cm}^{-1}$  (curve 1) and at 3363  $\text{cm}^{-1}$  (curve 2) are the characteristic absorption peaks for the –OH group in the phenolic resin. The peaks between 2950 and 2800  $\text{cm}^{-1}$  represent the absorption due to symmetrical and asymmetrical stretching of –CH group in the phenolic resin. The peaks in the range 1620–1454 are due to the –C=C stretching in the aromatic ring. The bending mode of vibration of –CH<sub>2</sub>– group resulted in the absorption at 1454 and 1375  $\text{cm}^{-1}$  (curve a); 1454 and 1381  $\text{cm}^{-1}$  (curve 2). The peak at 1261  $\text{cm}^{-1}$  (curve 1) is due to the absorption by C–O stretching. The stretching of ether linkage, C–O–C, is indicated by the absorption at 1009  $\text{cm}^{-1}$  (curve 1).

In curve 2, strong increase is observed for the intensity in the 1010 and 1251  $\text{cm}^{-1}$  in comparison with 1009 and 1261  $\text{cm}^{-1}$  of curve a respectively

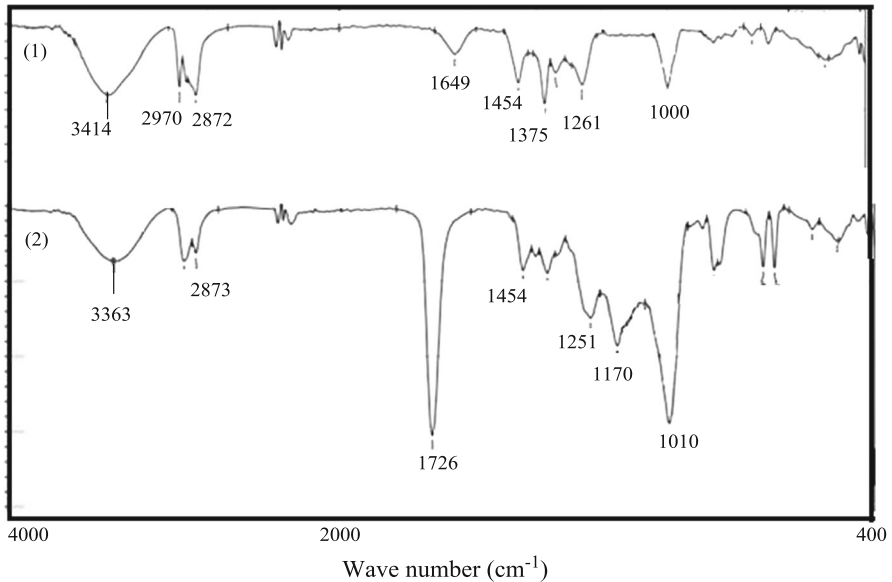


**Fig. 5** FTIR spectra of PR (1) and PR-ESO (2)

corresponding to the asymmetric stretch–shrink–vibrating peaks of phenol ether linkage, which means the phenol hydroxyl is etherified by ESO suggesting that the chemical reaction had happened between ESO and PR.

The proposed reaction mechanism between ESO and PR can be seen in Scheme 1. Normally, for the oxirane group located in the head of main chain the reaction between hydroxyl group and oxirane group can easily occur and don't need any other accelerator. However, in case of ESO the reaction between oxirane group and hydroxyl group hardly happen as result of low reactivity of oxirane group located in the middle of main chain so that need to use an accelerator. For this aim, NMI was used as an accelerator for reaction between hydroxyl group in phenol or phenolic resin and oxirane group in ESO. Firstly, the epoxy group was initiated by NMI to produce a zwitterion as shown in Scheme 1. A produced alkoxide anion reacts with hydroxyl group in phenol to give a ESO modified with phenol, which reacts with formalin to give phenolic resin.

### Mechanical properties

Tensile strength, flexible strength and izod impact strength of composite materials based on PR and PR-ESO with different contents of ESO were investigated. The results are shown in Figs. 6 and 7.

The effect of ESO contents on tensile properties, flexural strength, and impact strength are presented in both Figs. 6 and 7. The flexural strength, tensile strength and impact strength of the composite prepared with PR-ESO are higher than those of pristine phenolic resins, with maximum value at the 20 wt% ESO content.



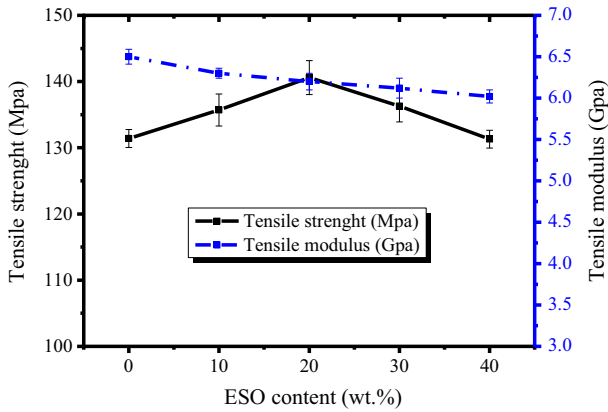


**Fig. 6** Effect of ESO content on tensile properties of composites

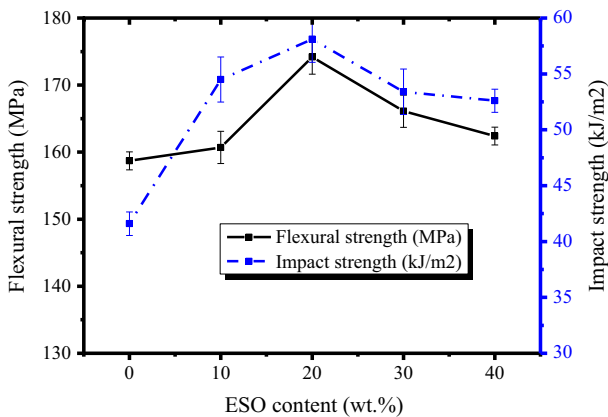


**Fig. 7** Effect of ESO contents on flexural strength and izod impact strength of composites

These results mean that the modification reaction with ESO helped to increase the mechanical strength of phenolic resins, resulting in increased flexural strength, tensile strength and impact strength of the composites based on PR-ESO. Namely, the tensile strength, flexural strength and impact strength of PR-ESO composites materials (20 wt% ESO) increased by 7.0, 20.5 and 39.7%, respectively, in comparison with unmodified PR composites. The modification reaction with ESO increases the ductility of phenolic resins, resulting in increased flexural strength [22]. Furthermore, the modification of phenolic resin with ESO helped the phenolic resin main chain to become longer and flexible. This is also the answer for the question why modified PR have higher impact strength when compared to pristine PR [5, 22]. The results in Fig. 6 also show that the cured PR seems to be softer with the presence of ESO than pristine PR as a result of decreasing in tensile modulus.

**Fig. 8** The interlaminar fracture toughness of PR (a, b) and PR-ESO (c, d) based composite materials

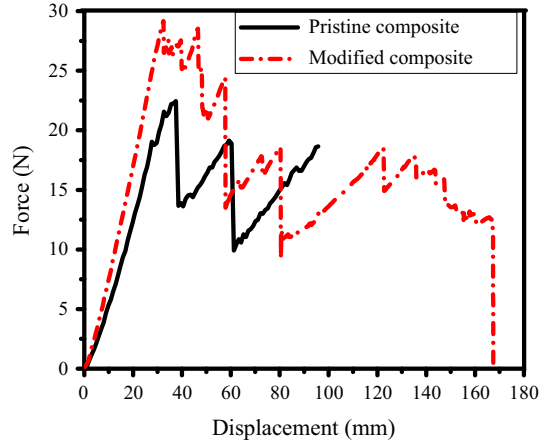


**Table 1**  $G_{IC}$  and  $G_{IP}$  of PR and PR-ESO composite materials

Sample	$G_{IC}$ (MBT), J/m <sup>2</sup>	$G_{IP}$ (MBT), J/m <sup>2</sup>
Pristine composite	217.5	259.6
PR-ESO (20 wt%)-based composite	387.8	478.9

### Effect of ESO to the mode I interlaminar fracture toughness of composite

The mode-I interlaminar fracture toughness of a GF/PR composite was determined using a double-cantilever beam test. The curves of the applied load versus displacement were recorded during the interlaminar fracture test and are shown in Fig. 8.

All the curves shown in Fig. 8 indicate that the force increased linearly until it reached a maximum, and then decreased, producing a zig-zag plot due to the difference between the resin-rich and fiber-rich regions along the longitudinal direction, that is, the voids and fractures of bridged fibers. An ESO content causes crack growth to be more stable and gradual than in the case of an unmodified specimen. In addition, with absence of ESO, the crack growth between two steps exhibits bad adhesion between each layer of a composite material. Both the force required to initiate a crack (maximum force in Fig. 8) and the force required to maintain the crack growth and displacement were higher with a ESO content than in the case of the unmodified composite. The results shown in Fig. 8 also show that a ESO content of 20 wt% in the epoxy matrix is the optimum value for attaining the maximum force as well as more stable crack growth.

The  $G_{IC}$  value corresponding to the initial crack initiation is determined from the load point at which the initiation of the delamination was microscopically observed at the edge of a specimen. Both the delamination initiation and delamination propagation mode-I fracture toughness values are shown in Table 1.

The delamination initiation ( $G_{IC}$ ) values were calculated from value of the first load peak of the R-curves, while the delamination propagation ( $G_{IP}$ ) values were taken from the plateau regions of the R-curves. As shown in Table 1, the  $G_{IC}$  and  $G_{IP}$  values of the composites with 20 wt% of ELO contents were higher than those of the unmodified composite. In addition, the propagation fracture values,  $G_{IP}$ , were higher than the initiation values,  $G_{IC}$ , due to toughening due to the likes of fiber bridging occurring only in the propagation state so that more energy was required to grow the crack further. Many mechanisms have been used to explain these results such as debonding between the fiber and resin, crack deflection, and fiber-bridging. However, it is not easy to identify the main mechanism. Normally, the mechanism enhancing the fracture toughness consists of more than one of the above-mentioned mechanisms [19, 29].

### Thermal stability

Conducted thermal analysis TGA with heating rate of 10 °C/min to measure the thermal resistance of PR and PR-ESO. Results are show in Fig. 9.

According to TGA of PR (Fig. 9, black line) and PR-ESO with 20 wt% ESO (Fig. 9, red line), both PR and PR-ESO start to decompose at about 350 °C. The decomposition process is almost entirely at a temperature of about 600 °C. Therefore, the thermal properties of ESO-PR resin are not much affected by the presence of ESO.

### SEM analysis

The scan electron microscope (SEM) of composite materials based on PR and ESO-PR are shown in Fig. 10. For the PR sample, the SEM image is smooth, brittle fracture surface, with almost no resin on the broken surface of the fiber. The PR-

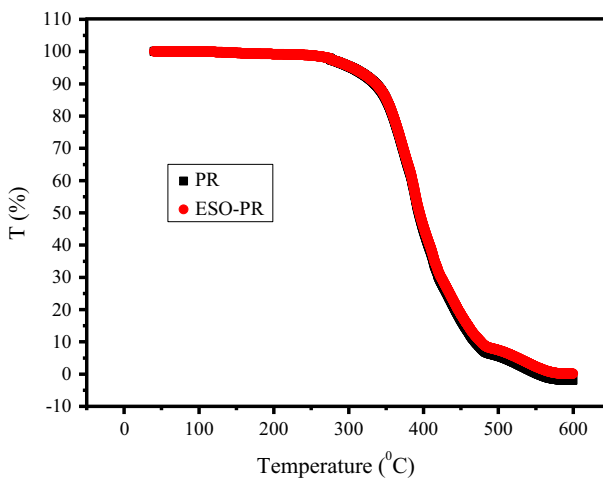


**Fig. 9** TGA diagrams of PR (black line) and PR-ESO (red line) (color figure online)

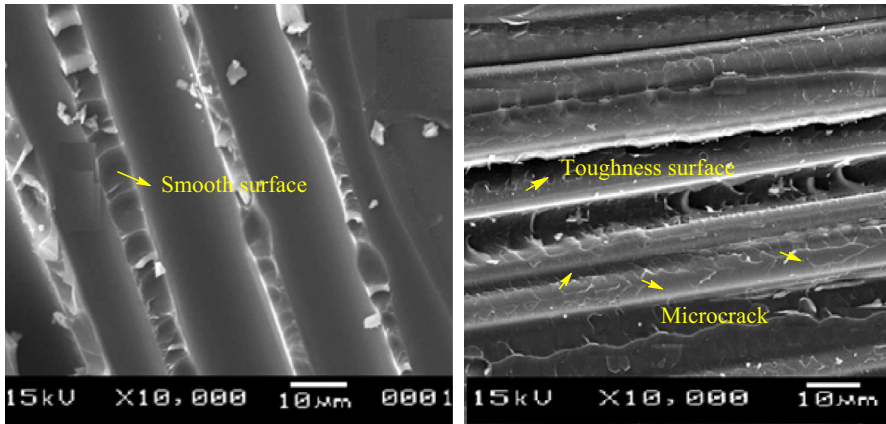


**Fig. 10** SEM images of fracture surfaces of composite materials based on PR and PR-ESO

ESO sample (20 wt% ESO) exhibits many small cracks on the surface, many irregular ridges and deformation lines in PF-ESO continuous phase. It means that the breaking process that takes place in the two materials is completely different and the main cause is the presence of ESO in the matrix.

## Conclusions

In this work, an ESO-PR-based composite with better mechanical properties and interlaminar fracture toughness in comparison with pristine PR-based composite was fabricated. The modification reaction of PR by using ESO is catalyzed by 1-methylimidazole. This process results in the grafting of ESO with phenolic resin. The best ESO content in order to obtain the highest toughening effect was 20 wt% based on the mass of phenol. At this ESO content, the tensile strength, flexural strength and impact strength of composites based on ESO-PR were improved by 7.0; 20.5 and 39.7%, respectively; and the toughness ( $G_{IC}$  and  $G_{IP}$ ) increased by 78.3 and 84.5%, respectively, in comparison with unmodified PR composites.

## References

1. Hirano K, Asami M (2013) Phenolic resins—100 years of progress and their future. *React Funct Polym* 73:256–269
2. Gardziella A, Pilato LA, Knop A (2000) Phenolic resins: chemistry, applications, standardization, safety and ecology, 2nd edn. Springer, New York
3. Morimoto T, Suzuki T, Iizuka H (2015) Wear rate and fracture toughness of porous particle-filled phenol composites. *Compos B Eng* 77:19–26

4. Hu Y, Geng W, You H, Wang Y, Loy DA (2014) Modification of a phenolic resin with epoxy- and methacrylate-functionalized silica sols to improve the ablation resistance of their glass fiber-reinforced composites. *Polymer* 6:105–113
5. Choi MH, Byun HY, Chung IJ (2002) The effect of chain length of flexible diacid on morphology and mechanical property of modified phenolic resin. *Polymer* 43:4437–4444
6. Abdalla MO, Ludwick A, Mitchell T (2003) Boron-modified phenolic resins for high performance applications. *Polymer* 44:7353–7359
7. Kaynak C, Cagatay O (2006) Rubber toughening of phenolic resin by using nitrile rubber and amino silane. *Polym Test* 25:296–305
8. Ma H, Wei G, Liu Y, Zhang X, Gao J, Huang F, Tan B, Song Z, Qiao J (2005) Effect of elastomeric nanoparticles on properties of phenolic resin. *Polymer* 46:10568–10573. <http://www.sciencedirect.com/science/journal/00323861>
9. Li C, Ma Z, Zhang X, Fan H, Wan J (2016) Silicone-modified phenolic resin: relationships between molecular structure and curing behavior. *Thermochim Acta* 639:53–65
10. Bu Z, Hu J, Li B (2014) Novel silicon-modified phenolic novolac resins: non-isothermal curing kinetics, and mechanical and thermal properties of their biofiber-reinforced composites. *Thermochim Acta* 575:244–253
11. Li S, Han Y, Chen F, Luo Z, Li H, Zhao T (2016) The effect of structure on thermal stability and anti-oxidation mechanism of silicone modified phenolic resin. *Polym Degrad Stab* 124:68–76
12. Nair CPR (2004) Advances in addition-cure phenolic resins. *Prog Polym Sci* 29:401–498
13. Ma H, Wei G, Liu Y, Zhang X, Gao J, Huang F, Tan B, Song Z, Qiao J (2005) Effect of elastomeric nanoparticles on properties of phenolic resin. *Polymer* 46:10568–10573
14. Megiatto JD Jr, Ramires EC, Frolini E (2010) Phenolic matrices and sisal fibers modified with hydroxy terminated polybutadiene rubber: impact strength, water absorption, and morphological aspects of thermosets and composites. *Ind Crops Prod* 31:178–184
15. Nayak RK, Ray BC (2017) Water absorption, residual mechanical and thermal properties of hydrothermally conditioned nano-Al<sub>2</sub>O<sub>3</sub> enhanced glass fiber reinforced polymer composites. *Polym Bull* 74:4175–4194
16. Behrooz FT, Maher BM, Shokrieh MM (2015) Mechanical properties modification of a thin film phenolic resin filled with nano silica particles. *Comput Mater Sci* 96:411–415
17. Ren G, Zhang Z, Song Y, Li X, Yan J, Wang Y, Zhu X (2017) Effect of MWCNTs-GO hybrids on tribological performance of hybrid PTFE/Nomex fabric/phenolic composite. *Compos Sci Technol* 146:155–160
18. Vu CM, Sinh LH, Choi HJ, Pham TD (2017) Effect of micro/nano white bamboo fibrils on physical characteristics of epoxy resin reinforced composites. *Cellulose* 24:5475–5486
19. Vu CM, Nguyen DD, Sinh LH, Pham TD, Pham LT, Choi HJ (2017) Environmentally benign green composites based on epoxy resin/bacterial cellulose reinforced glass fiber: fabrication and mechanical characteristics. *Polym Test* 61:150–161
20. Vu CM, Nguyen DD, Sinh LH, Choi HJ, Pham TD (2017) Micro-fibril cellulose as a filler for glass fiber reinforced unsaturated polyester composites: fabrication and mechanical characteristics. *Macromol Res*. <https://doi.org/10.1007/s13233-018-6006-3>
21. Hoang SL, Vu CM, Pham LT, Choi HJ (2017) Preparation and physical characteristics of epoxy resin/bacterial cellulose biocomposites. *Polym Bull*. <https://doi.org/10.1007/s00289-017-2162-4>
22. Yue S, Jianfeng H, Hang H, Heqing F, Hanwei Z, Huanqin C (2007) Synthesis, properties and application of a novel epoxidized soybean oil-toughened phenolic resin. *Chin J Chem Eng* 15:418–423
23. Situ Y, Hu J, Huang H, Fu H, Zeng H, Chen H (2008) Synthesis and application of phenolic resin internally toughened by chain extension polymer of epoxidized soybean oil. *Front Chem China* 3:235–241
24. Kumar S, Samal SK, Mohanty S, Nayak SK (2017) Epoxidized soybean oil-based epoxy blend cured with anhydride-based cross-linker: thermal and mechanical characterization. *Ind Eng Chem Res* 56:687–698
25. Roudsari GM, Mohanty AK, Misra M (2014) Study of the curing kinetics of epoxy resins with biobased hardener and epoxidized soybean oil. *ACS Sustain Chem Eng* 2:2111–2116
26. Kumar S, Samal SK, Mohanty S, Nayak SK (2017) Study of curing kinetics of anhydride cured petroleum-based (DGEBA) epoxy resin and renewable resource based epoxidized soybean oil (ESO) systems catalyzed by 2-methylimidazole. *Thermochim Acta* 654:112–120

27. Sinclair RG, McKay AF, Jones RN (1952) The infrared absorption spectra of saturated fatty acids and esters. *J Am Chem Soc* 74:2570–2575
28. Colthup NB, Day LH, Wiberley SE (1990) *Introduction to infrared and Raman spectroscopy*, 3rd edn. Academic Press, San Diego
29. Vu CM, Nguyen TV, Nguyen LT, Choi HJ (2016) Fabrication of adduct filled glass fiber/epoxy resin laminate composites and their physical characteristics. *Polyme Bull* 73:1373–1391